Research article

Multi-objective atom search optimization of biodiesel production from palm empty fruit bunch pyrolysis

Rawinun Junsittiwate [a], Thongchai Rohitatisha Srinophakun [a,*], Somboon Sukpancharoen [b]

[a] Department of Chemical Engineering, Center for Advanced Study in Industrial Technology, Faculty of Engineering, Kasetsart University, Bangkok, 10900, Thailand
[b] Division of Mechatronics and Robotics Engineering, Rajamangala University of Technology Thanyaburi, Pathum Thani, 12110, Thailand

HIGHLIGHTS

- Biodiesel production from palm empty fruit bunch pyrolysis.
- An optimum condition by central composite design.
- Multi-objective optimization using atom search optimization.

ARTICLE INFO

ABSTRACT

In this study, palm empty fruit bunch (PEFB) pyrolysis, bio-oil improvement, and generating electricity were all simulated using Aspen plus. This research employed a kinetic reactor for pyrolysis at 500 °C based on 1,000 tons of PEFB per day. The simulation results indicated that 1 kg/hr. PEFB generated 0.11 kg/hr of char, 0.21 kg/hr of gas, and 0.67 kg/hr of bio-oil, which is in good agreement with literature. The relationship between biodiesel yield, CO_2 emissions, and utility costs was then investigated the effect of the distillate-to-feed ratio of biodiesel distillation, heat exchanger temperature, and the flash drum pressure from the process simulation by using central composite design (CCD). The coefficient of determination (R^2) values for biodiesel yield, CO_2 emissions, and utility costs were 0.9940, 0.9941, and 0.9959, respectively, which was a reason for the excellent model fitting. The optimum response (the biodiesel yield, the CO_2 emission, and the utility cost) was obtained at 5,562.73 kg/hr, 33,696.55 kg/hr, and 2,953.99 USD/hr., respectively, with optimum conditions for the distillate-to-feed ratio of 0.899999, temperature of 56.0356 °C and pressure of 18.1479 bar. After that, a quadratic polynomial equation from the RSM was employed as the fitness function to evaluate the fitness value of the multi-objective optimization (MOO) by atom search optimization (ASO) to maximize biodiesel yield and minimize the CO_2 emissions and utility costs. The ASO performance was generated into the Pareto optimal solution of 200 generations. The optimal CCD was then compared with the ASO results. It was found that the ASO could reduce CO_2 emissions by 1.33% and reduce utility costs by 5.03% while increasing biodiesel yields by 7.01%. It can be observed that the ASO was more efficient at finding parameters than the CCD.

1. Introduction

Palm oil is a major agricultural commodity in Thailand. In 2020, about 6.3 million rai of plantations produced oil palm, which harvested 15.65 million tons [1]. The residue from industrial palm oil manufacturing includes palm empty fruit bunch (PEFB), which has a high volume of up to 22% of fresh bunch weight; this country produces over one million tons of PEFB per year. The main components of PEFB comprise hemicellulose 20.58–33.52%, cellulose 23.7–65%, and lignin plus others 14.1–30.45% [2]. Cellulose, hemicellulose, and lignin can produce bio-oil.

Pyrolysis is the heat degradation of a substance with the lack of oxygen, causing decomposition investigated with the chemical characteristics of the element by an endothermic reaction yielding bio-oil, gas, and char [3]. For maximum liquid output, biomass pyrolysis temperatures should be between 400 and 550 °C. Liquid and char are converted to gas at elevated temperatures because of increased breaking reactions. The residence time of the produced smoke remaining at the pyrolysis

temperature is referred to as the residence time of hot vapors. In pyrolysis, a short residence time for liquid products is desirable because it reduces secondary reactions. Increased residence time reduces pyrolysis liquid yield while increasing pyrolytic gas yield. The residence time of fluidized bed reactors can be reduced to less than 1 s [4].

Response surface methodology (RSM) is a set of mathematics methods, statistics for modeling and evaluating issues in which several factors affect the response of interest to optimize the response. Consequently, the central composite design (CCD) output was assessed employing RSM [5]. To investigate the quadratic responses and squared terms of the preparatory variables, quadratic polynomial equations were created. The CCD statistical design of studies was used to collect the most important data about a process using a limited amount of tests. Particularly, the CCD involves applying the second-order model in an effective method. This work was applied to optimize by RSM of a biodiesel power plant derived from a palm empty fruit bunch [6].

Multi-objective optimization (MOO) can optimize efficiency by choosing the operating conditions and adding desired outcome measures (or minimizing unwanted amounts). The process for the proposed approach entails determining the selection issue aims, objective functions, and constraints. In general, there is a better collection of solutions for one or more objectives in MOO issues than in other areas. This solution is called Pareto-optimal solutions or non-dominated solutions [7, 31]. Sukpancharoen et al. [8] conducted this study by the CCD to obtain the optimal scenario for MOO by a Gray Wolf optimizer technique. Comparison was performed using a Spotted Hyena optimizer to solve the combined cycle power plants by using single-objective and MOO [9].

Atom Search Optimization (ASO) is a novel optimization technique motivated by a molecular force that provides additional benefits when dealing with complex global optimization issues. Many academics have been interested in ASO because of its beneficial properties. The hydrogeological parameter estimation issue suggested ASO by Zhao et al. [10] in 2019. The results showed ASO improves unimodal functions and competes well in multimodal functions. Based on several types of benchmark functions, ASO achieves a superior self-adaptive convergence. ASO is straightforward to implement due to its simplicity and minimal control options. Almagboul et al. [11] used ASO to lower the

maximum level of the beam pattern's side-lobe and guide the null in the desired direction. Agwa et al. [12] employed ASO to mimic steady-state fuel cells.

The motivation for the connection between CCD and ASO is because CCD helps to estimate the curvature in the response that is continuously obtained. It can reduce the number of tests that can be developed in variables. In response to surface modelling and optimization, it is commonly used [13]. Despite its numerous benefits, it cannot be used to optimize all operations, since it can only produce second-order equations, which is a limitation. Furthermore, the information would be better used with other methods. ASO algorithms can also be adapted to the specifics of a problem, resulting in better efficiency and convergence than a box or points in the cube. The ASO method is a higher-level procedure that generates an estimated solution in parameter space that is too enormous to be explored completely, such as surface region [14].

The purpose of using the RSM optimization method (CCD) in combination with MOO-ASO was to determine the optimal distillation-to-feed ratio, temperature, and pressure parameters for the biodiesel process. The RSM was then used to create a quadratic polynomial equation. It described the correlation between the process variables and the output response; the RSM model was used as a fitness function to enable the ASO algorithm to find the optimal parameter. This was performed to minimize the objective function, and optimize biodiesel production by reducing (CO_2 emissions and utility costs).

2. Materials and methods

2.1. Process description

The entire procedure is presented in Figure 1. In the first step, PEFB is fed into the pretreatment section for drying and crushing. Next, the dried PEFB is conveyed to the pyrolysis section to generate bio-oil, char, and gas. Next, the pyrolysis product is sent for solid removal and bio-oil recovery to separate char and gas. The gas and char go to combustion, while hydroprocessing is used to upgrade the bio-oil. Hydroprocessing is required. Finally, the flue gas is used for electric generation [15].
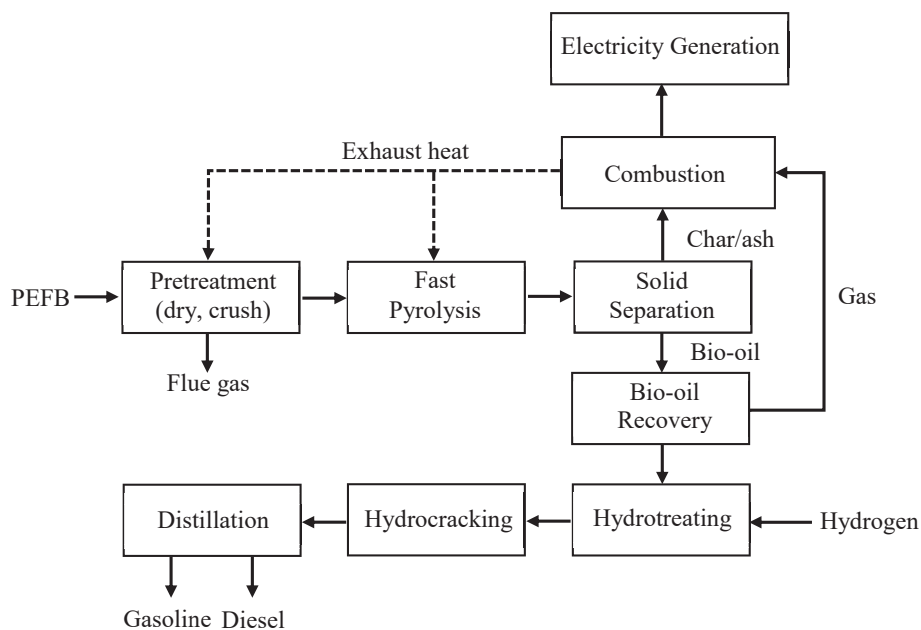

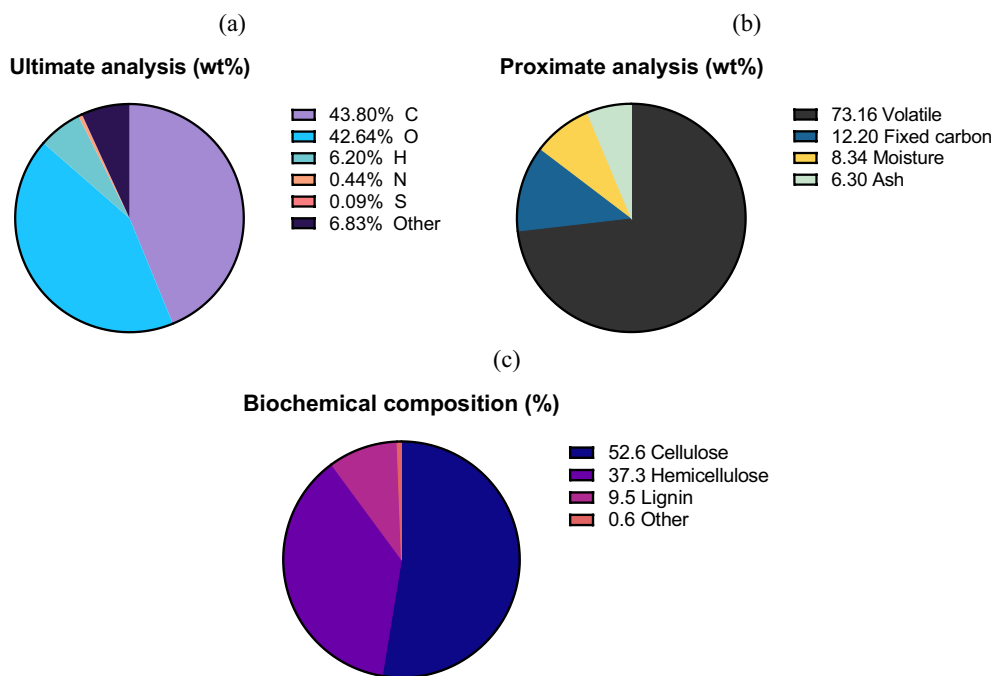**Figure 1.** Block diagram for bio-oil process and upgrading.

Figure 2. Composition of PEFB in Thailand (a) ultimate analysis, (b) proximate analysis, (c) biochemical composition.

2.2. Process simulation

The biodiesel production from PEFB is implemented in Aspen Plus V11. Figure 2 (a-c) shows the key parameter estimates utilized in this investigation. The carbon from ultimate analysis of PEFB is 43.80 %, while the volatile from proximate analysis is 73.16% and biochemical composition is determined of cellulose 52.60% [16].

Figure 3 shows the results of the Aspen Plus V11 simulation on bio-oil production and upgrading with a heat exchanger network design. PEFB was fed into the process at a mass flow rate of 1,000 tons/day. The first step was to pre-treat the PEFB to reduce its size to about 3 mm, then dry it to less than 10% moisture content. The reactor (CSTR) was operated at 500 °C at a residence time of 1 s. The pyrolysis model used 149 kinetic equations to decompose PEFB into char, gas, and bio-oil [17]. A cyclone was then used to separate the biochar. The volatile product was a direct mixed bio-oil stream quenched to 100 °C, and 45 °C to avoid pyrolysis. A gas turbine was used to generate electricity. The combustor was modeled as two
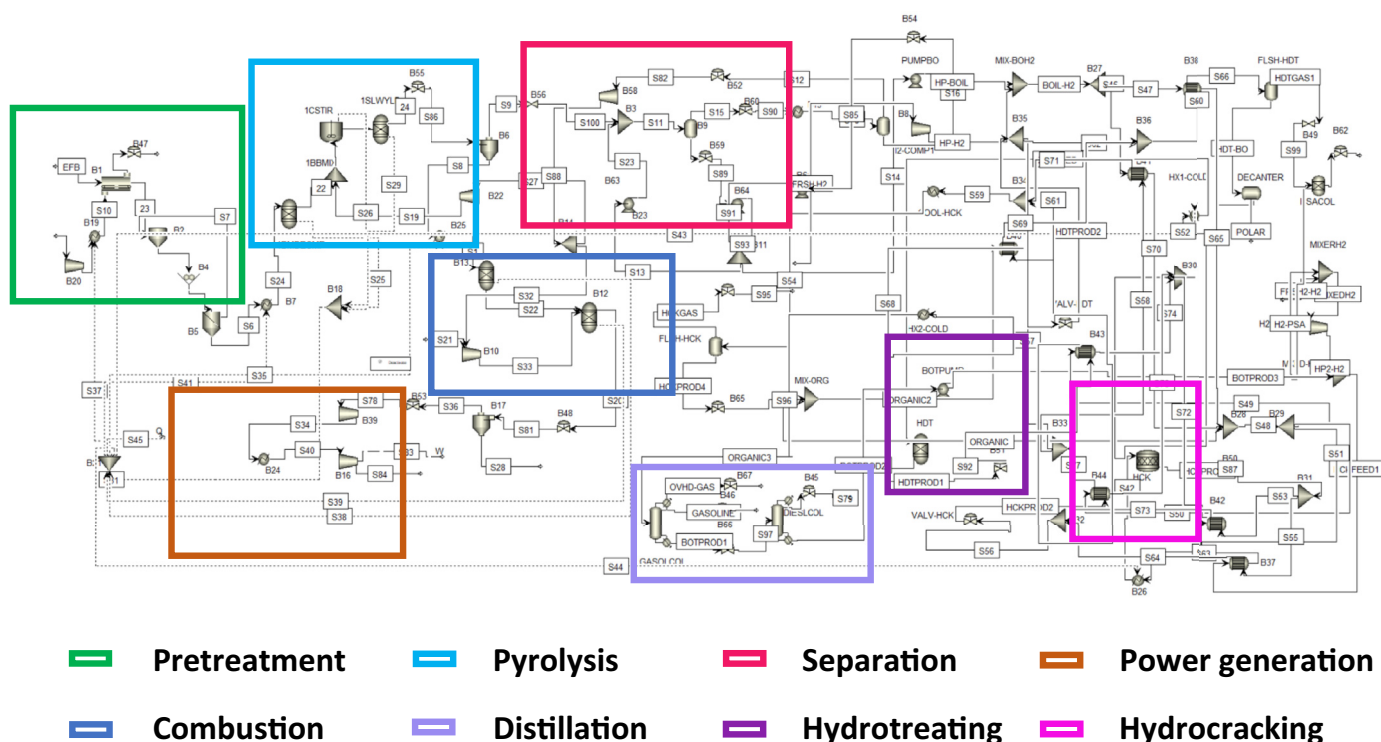

Figure 3. Process flow diagrams for bio-oil process and bio-oil upgrading with a heat exchanger network design.

Factors	Levels				
	-1.68	-1	0	1	1.68
A = distillate-to-feed ratio	0.6989	0.75	0.825	0.9	0.9511
B = temperature (°C)	6.36	20	40	60	73.64
C = pressure (bar)	8.18	15	25	35	41.82

reactors (RYield and RGibbs) that calculate heat balance and combustion products by using Gibbs energy minimization. The gas from the combustor was used to generate the electricity by a gas turbine. Bio-oil is thermally unstable and has a low density owing to its increased oxygen levels. As a result, there is a need for an upgrade. The hydrotreated yields were adjusted to an oxygen content of less than 2% by using high hydrogen pressure at 87 bar and a WHSV of 0.135 h^{-1}. The hydrotreated bio-oil separated the gas and polar components before the two distillation columns were distilled into gasoline, diesel, and heavy residue. The second column's heavy compounds were cracked into smaller hydrocarbons within the desired boiling range of the hydrocracker. The hydrocracker was developed in RStoic from [18] work, which obtains six reactions. The heat exchanger network was used to minimize the energy consumption of the process. The Aspen Energy Analyser V11 has been recommended in 10 designs. The selected design had the lowest total cost [19].

2.3. Design of the process simulation

This research aimed to maximize biodiesel yield while minimizing CO_2 emissions and utility costs selected as the response values. The primary parameters that have a significant impact on the defined response were presented as independent variables. One of the most promising processes for separating biodiesel and CO_2 from the mixing stream was the distillation section. Therefore, the distillate-to-feed ratio was chosen as one variable to match the distillation column specifications. The pressure of the flash drum (FLSH-HDT) and the temperature of the heat exchanger (B38) were chosen as independent variables for the other two variables. Light hydrocarbons (C1–C4) and H_2 gas were removed from the hydrotreated stream using these two devices. According to the study [20], the light hydrocarbons acted as a toxic compound in bio-oil production. The other parameters, except for the independent factors, were assumed to have a constant value. The levels using CCD were entered into the Design-Expert V13 (trial) after specifying the levels of the coded in Eq. (1), and the range of values as shown in Table 1.

$$Y = \beta_0 + \sum_{i=1}^{n} \beta_i X_i + \sum_{i=1}^{n} \beta_{ii} X_i^2 + \sum_{i=1}^{n} \sum_{j>1}^{n} \beta_{ij} X_i X_j \tag{1}$$

where β_o, β_i, β_{ii}, and β_{ij} are the correlation coefficients for the fixed, linear, nonlinear, and interactive components, respectively; and Y is the expected system output. The coded independent factors are designated by the labels X_i and X_j. The model's sufficiency is checked as the final stage. Testing the lack of fit is one technique for accomplishing this goal.
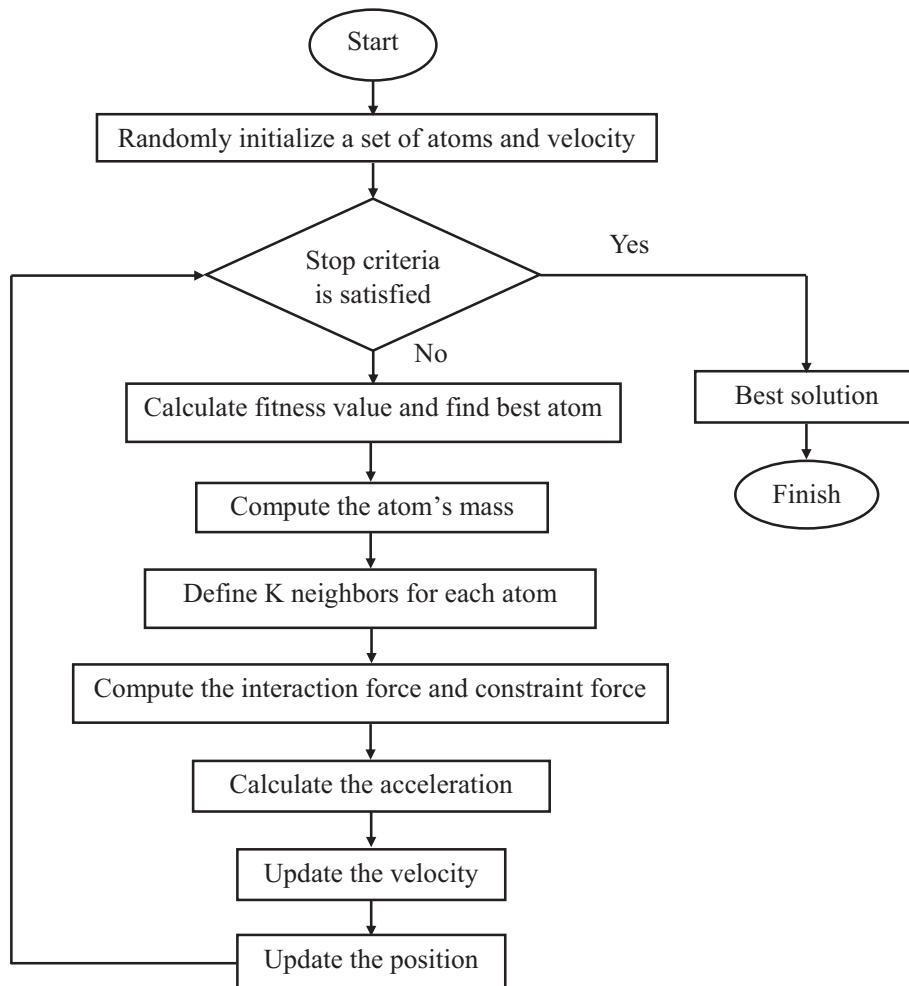

Figure 4. The ASO algorithm flowchart.

A lack of fit is a metric for how well a model represents simulation process data [21].

ASO is a recently devised optimization algorithm based on basic molecular dynamics and has been discussed. Only the most essential formulas will be presented [10]. The atoms' positions are updated in the ASO by Eq. (2).

$$x_i^d(t+1) = x_i^d(t) + v_i^d(t+1) \tag{2}$$

where $x_i^d(t)$ represents the location of the i atomic in the t iteration, $x_i^d(t+1)$ means the location of the i atomic in the $(t+1)$ step, and $v_i^d(t+1)$ denotes the i atom's velocity in the $(t+1)$ iteration computed from Eq. (3).

$$v_i^d(t+1) = rand_i^d v_i^d(t) + a_i^d(t) \tag{3}$$

where rand is an integer randomly selected from the range [0, 1], and $a_i^d(t)$ is the acceleration of the i atomic in the t iteration, which was calculated by Eq. (4).

Total force is written as the total of elements with weights randomly in the d dimension acting on the atomic mass i of the other atomic mass in Eq. (7).

$$F_i^d(t) = \sum_{j \in Kbest} rand_j F_{ij}^d(t) \tag{7}$$

where $rand_j$ is an integer between 0 and 1.

The constraint effort might be obtained by Eq. (8).

$$G_i^d(t) = \lambda(t)\left(x_{best}^d(t) - x_i^d(t)\right) \tag{8}$$

where $\lambda(t)$ denotes the Multiplier Lagrangian.

$K(t)$ is a reducing time function as the iteration number rises, and it can be determined as Eq. (9).

$$K(t) = N - (N-2) \times \sqrt{\frac{t}{T}} \tag{9}$$

where N denotes the amount of atoms. The ASO algorithm's flowchart is

$$a_i^d(t) = \frac{F_i^d(t)}{m_i^d(t)} + \frac{G_i^d(t)}{m_i^d(t)} = -\propto \left(1 - \frac{t-1}{T}\right)^3 e^{-\frac{20t}{T}} \sum_{j \in Kbest} \frac{rand_j\left(2 \times \left(h_{ij}(t)\right)^{13} - \left(h_{ij}\right)^7\right)}{m_i(t)} \frac{\left(x_i^d(t) - x_i^d(t)\right)}{x_i(t), x_i(t)_2} + \beta e^{-\frac{20t}{T}} \frac{x_{best}^d(t) - x_i^d(t)}{m_i(t)} \tag{4}$$

where $m_i(t)$ represents the mass of the i atomic at the t iteration, which could be calculated by using its function fitness at the most basic level. Where $\propto = 50$ and $\beta = 0.2$.

The higher the function fitness, the more mass the atom, which slows it down. The i atom's mass can be computed by using the Eqs. (5) and (6).

$$M_i(t) = e^{\frac{Fit_i(t) - Fit_{best}(t)}{Fit_{worst}(t) - Fit_{best}(t)}} \tag{5}$$

$$m_i(t) = \frac{M_i(t)}{\sum_{j=1}^{N} M_j(t)} \tag{6}$$

shown in Figure 4.

2.4. Weighted-sum multi-objective function

The relevance of multiple objectives can be explained using weight coefficients. As a consequence, a weighted sum decision-making approach was employed to identify the trade-off solution from the Pareto set [22]. The following is the equation for the weighted-sum objective function $(F(x))$ with Eq. (10).

$$F(x) = w_1/f_1 + w_2 f_2 + w_3 f_3 \tag{10}$$

Table 2. Simulation process matrix for CCD with defined response values.

Run No.	Level of factors employed			Responses		
	A (-)	B (°C)	C (bar)	Y_1 (kg/hr.)	Y_2 (kg/hr.)	Y_3 (USD/hr.)
1	0.9	60	35	5,886.42	33,697.6	2,947.44
2	0.9	20	35	6,430.72	34,522.6	3,120.32
3	0.75	60	35	5,406.77	34,050.1	2,997.67
4	0.825	40	25	5,775.91	34,383.5	3,071.52
5	0.951134	40	25	6,166.51	33,880.5	3,007.09
6	0.825	40	8.18207	5,344.44	34,257.8	3,053.66
7	0.825	40	41.8179	6,043.18	34,454.7	3,082.21
8	0.75	20	35	5,905.68	34,827.6	3,169.12
9	0.9	20	15	6,010.24	34,374.4	3,097.30
10	0.9	60	15	5,427.13	33,579.0	2,932.88
11	0.825	6.36414	25	6,142.94	34,934.1	3,188.09
12	0.825	73.6359	25	5,022.10	33,446.6	2,879.81
13	0.75	60	15	4,984.68	33,951.4	2,981.84
14	0.825	40	25	5,775.91	34,383.5	3,071.52
15	0.75	20	15	5,518.47	34,718.5	3,147.40
16	0.698866	40	25	5,324.75	34,594.9	3,118.64

where A = distillate to feed ratio of biodiesel column, B = temperature of heat exchanger (°C), C = pressure of flash drum (bar), Y_1 = biodiesel yield (kg/hr), Y_2 = CO_2 emission (kg/hr), Y_3 = utility cost (USD/hr).

w = weighted measure, where w_1 = 3,300 for productivity, w_2 = 3,300 for environment, and w_3 = 3,300 for economic objective.

The lower boundary of x_i = [0.698866 6.36414 8.18207]

The upper boundary of x_i = [0.951134 73.6359 41.8179] where x_1 is the mass to distillate ratio of the biodiesel column.

x_2 is the temperature of COOL-HDT (°C).

x_3 is the pressure of FLSH-HDT (bar).

Table 3. ANOVA analysis of biodiesel yield.

Source	Sum of Squares	Degree of Freedom	Mean Square	F-value	p-value	
Model	2.666E+06	9	2.962E+05	110.65	<0.0001	significant
A	8.240E+05	1	8.240E+05	307.79	<0.0001	
B	1.198E+06	1	1.198E+06	447.55	<0.0001	
C	6.007E+05	1	6.007E+05	224.38	<0.0001	
AB	1,121.44	1	1121.44	0.4189	0.5414	
AC	620.93	1	620.93	0.2319	0.6472	
BC	678.78	1	678.78	0.2535	0.6325	
A^2	153.99	1	153.99	0.0575	0.8184	
B^2	35,319.94	1	35,319.94	13.19	0.0109	
C^2	4,647.83	1	4,647.83	1.74	0.2357	
Residual	16,063.07	6	2,677.18			
Lack of Fit	16,063.07	5	3,212.61			
Pure Error	0	1	0			
Cor Total	2.682E+06	15				

Table 4. ANOVA analysis of CO_2 emissions.

Source	Sum of Squares	Degree of Freedom	Mean Square	F-value	p-value	
Model	2.956E+06	9	3.285E+05	112.42	<0.0001	significant
A	4.857E+05	1	4.857E+05	166.22	<0.0001	
B	2.351E+06	1	2.351E+06	804.77	<0.0001	
C	47,527.26	1	47,527.26	16.27	0.0069	
AB	718.59	1	718.59	0.2459	0.6376	
AC	435.50	1	435.50	0.1491	0.7128	
BC	198.36	1	198.36	0.0679	0.8031	
A^2	34,051.05	1	3,4051.05	11.65	0.0143	
B^2	55,427.16	1	55427.16	18.97	0.0048	
C^2	3,237.97	1	3237.97	1.11	0.3330	
Residual	17,530.83	6	2921.80			
Lack of Fit	17,530.83	5	3506.17			
Pure Error	0	1	0			
Cor Total	2.974E+06	15				

Table 5. ANOVA analysis of utility costs.

Source	Sum of Squares	Degree of Freedom	Mean Square	F-value	p-value	
Model	1.183E+05	9	13142.11	162.14	<0.0001	significant
A	10892.74	1	10892.74	134.39	<0.0001	
B	1.042E+05	1	1.042E+05	1285.29	<0.0001	
C	1110.58	1	1110.58	13.70	0.0101	
AB	0.0116	1	0.0116	0.0001	0.9908	
AC	0.0001	1	0.0001	1.003E-06	0.9992	
BC	25.73	1	25.73	0.3175	0.5936	
A^2	159.04	1	159.04	1.96	0.2108	
B^2	1912.75	1	1912.75	23.60	0.0028	
C^2	51.21	1	51.21	0.6318	0.4570	
Residual	486.31	6	81.05			
Lack of Fit	486.31	5	97.26			
Pure Error	0	1	0			
Cor Total	1.188E+05	15				

f_1 is the maximum yield of biodiesel in kg/hr.
f_2 is the minimum of CO_2 emission in kg/hr.
f_3 is the minimum utility cost in USD/hr.

3. Results and discussion

This work used a plant size of 1,000 tons per day, with the results presented as kg/hr. PEFB generated 0.11 kg/hr of char, 0.21 kg/hr of gas, and 0.67 kg/hr of bio-oil, which was in good agreement with the literature [16]. The base case condition of the distillate-to-feed ratio was 0.51, heat exchanger temperature of 50 °C, flash drum pressure of 20 bar [17], and an output volume of 3,443.96 kg/hr for diesel, CO_2 emission of 35,102.58 kg/hr, and a utility cost of 3,224.92 USD/hr. The power generation capacity was approximately 0.28 MW. The result of the heat exchanger network showed a total cost of around 810,974.55 USD/year. We installed more heat exchangers to bring the process to a back heating process and saved 70.83% of the added heating or cooling energy load and a 57.46% reduction in the total cost.
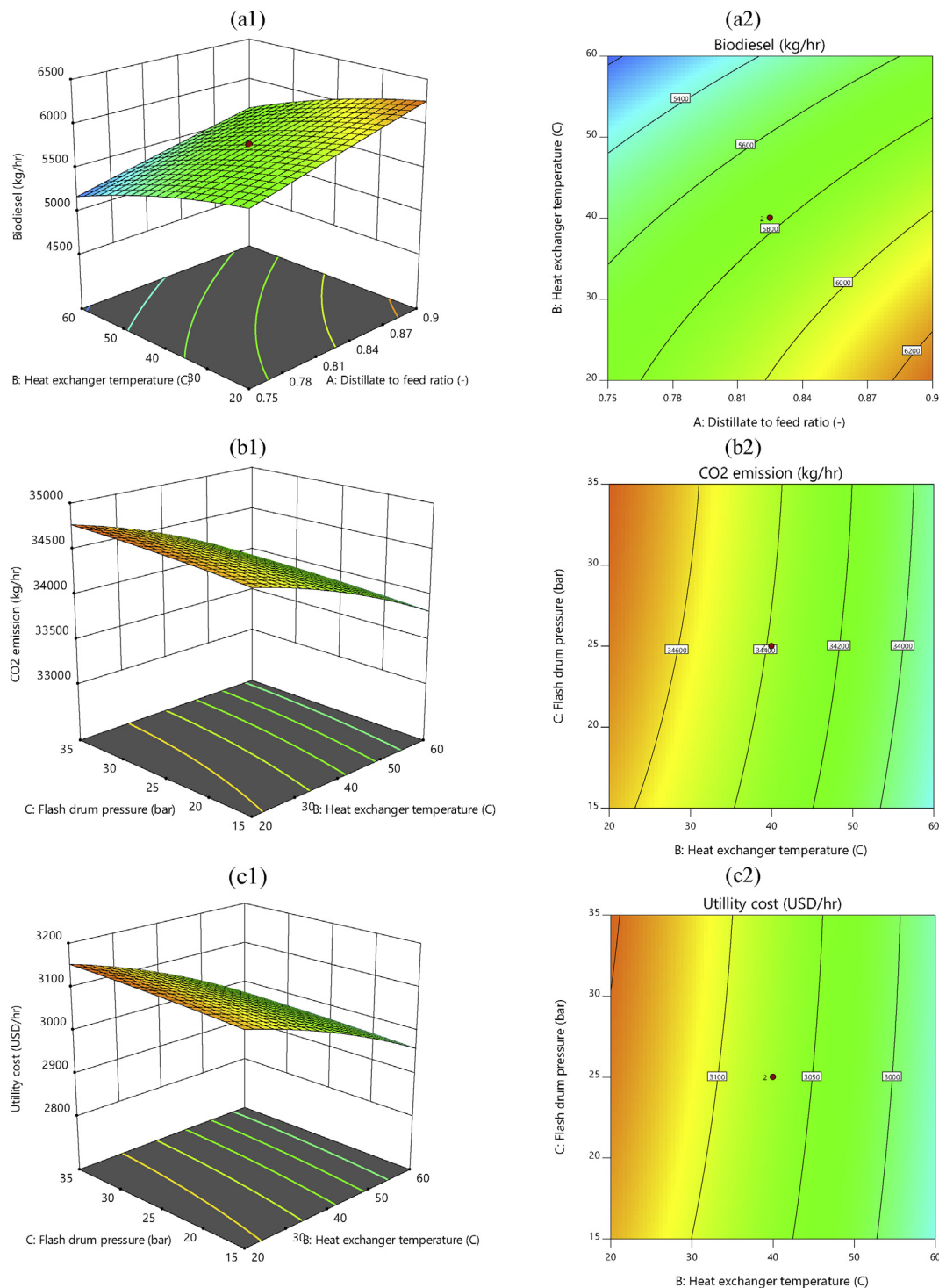

Figure 5. Response surface and contour plots (a1 and a2) effect of heat exchanger temperature and distillate-to-feed ratio on biodiesel yield, (b1 and b2) flash drum pressure and the heat exchanger temperature on CO_2 emissions, (c1 and c2) effect of flash drum pressure and heat exchanger temperature on utility costs.
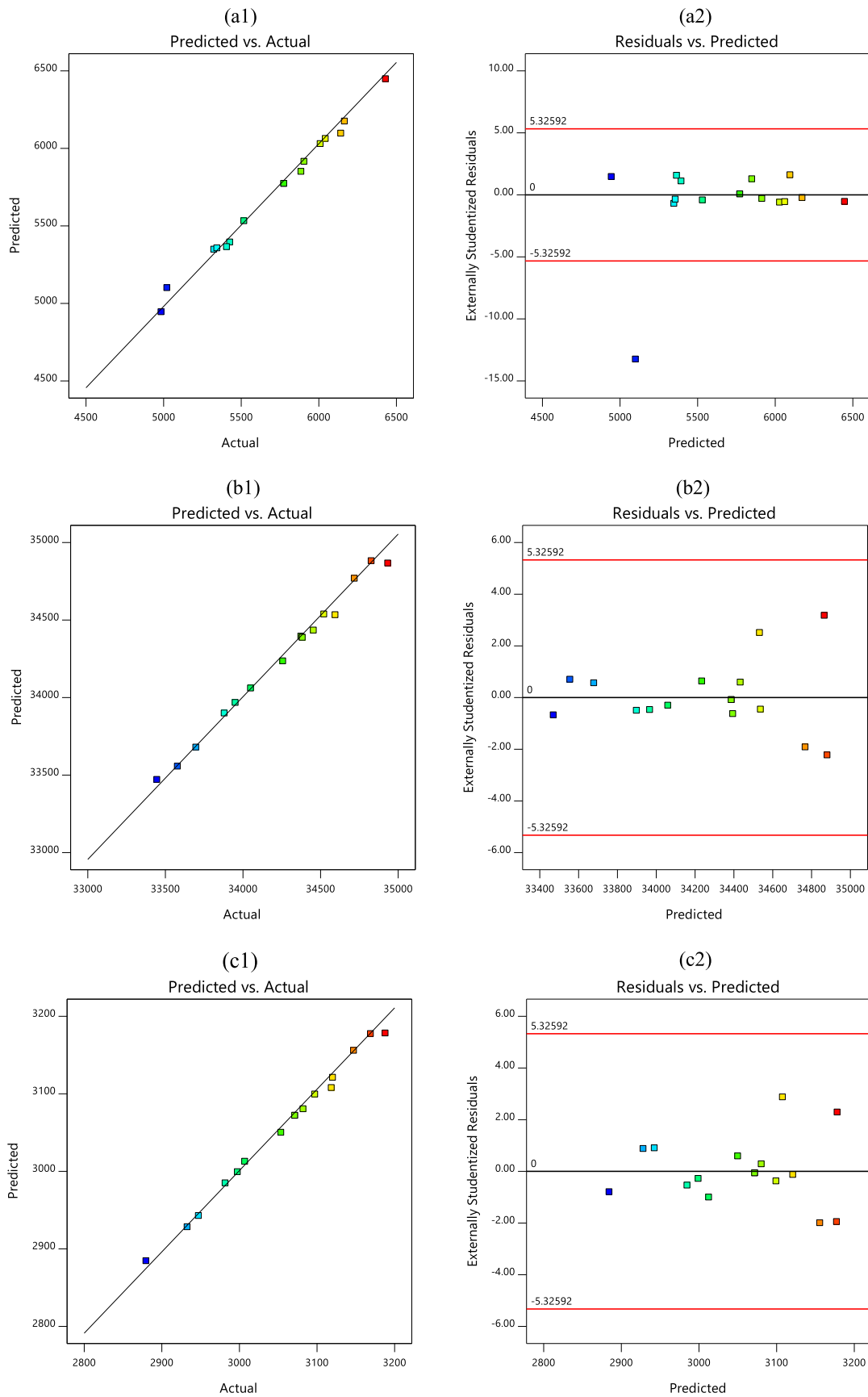
Figure 6. Relationship between predicted versus actual values and studentized residuals for (a1 and a2) biodiesel yield, (b1 and b2) CO_2 emission, and (c1 and c2) utility cost.

Design Experts software V13 (trial) proposed 16 simulation process runs of formulations for the CCD, as shown in Table 2. The distillate-to-feed ratio of the biodiesel column (A), the temperature of the heat exchanger [B38] (B), and the pressure of the flash drums [FLSH-HDT] (C) are the three factors studied. To design the characteristic model, the study examined the varied effects of the independent components on biodiesel yield (kg/hr.), CO_2 emissions (kg/hr.), and utility costs (USD/hr.).

The adjustment of the quadratic model was evaluated by using ANOVA [23], and the results are presented in Tables 3, 4, and 5. These model terms were significant if the P-value is lower than 0.05 with a confidence level of 95% [24]. Biodiesel yield, CO_2 emission, and utility cost models were all determined to be significant, with an R^2 of 0.9940, 0.9941, and 0.9959, respectively. The results were influenced by the ratio of a distillation column, heat exchanger temperature, and flash drum pressure. The heat exchanger and flash drums conditions were relevant to the product yield and cost, which influenced the phase separation of the product. The effect of the distillate-to-feed ratio on product purity was also observed [20].

Table 3 indicates a model F-value of 110.65 for biodiesel and a P-value of less than 0.05, which indicates that the model equation is significant. The model F-value of 112.42 for CO_2 emission in Table 4 and the P-value of less than 0.05 indicate that the equation for CO_2 emissions is significant. The lack of fit F-value of 17,530.83 indicates a significant correlation interrelated to the pure error [25]. Likewise, ANOVA analyses of the utilities are shown in Table 5. The F-value of 162.14 and p-value below 0.05 represent significant utility cost equations, where the high F-value indicates the potential for interference at only 0.01% of noise [26].

The second-order mathematical model was developed in Eqs. (11), (12), and (13) for the predictive biodiesel yield (Y_1), CO_2 emission (Y_2), and utility cost (Y_3), respectively:

$$Y_1 = 2{,}286.84308 + 4{,}493.09824A + 2.89972B + 20.63873C - 7.89317AB + 11.74667AC + 0.046056BC - 724.80237A^2 - 0.143655B^2 - 0.223987C^2 \quad (11)$$

$$Y_2 = 29{,}351.51730 + 15{,}276.16768A + 0.558043B + 8.12684C - 6.31837AB + 9.83753AC - 0.024897BC - 10{,}778.0574A^2 - 0.193374B^2 - 0.186954C^2 (12)$$

$$Y_3 = 2{,}951.52074 + 839.74564A - 1.248B + 2.43247C - 0.025407AB + 0.004251AC - 0.008967BC - 736.60224A^2 - 0.035922B^2 - 0.0023510C^2 (13)$$

Increasing the distillate-to-feed ratio (0.75–0.9) increases the biodiesel yield (4,500 to 6,500 kg/hr) as illustrated in Figure 5a1 and a2. In
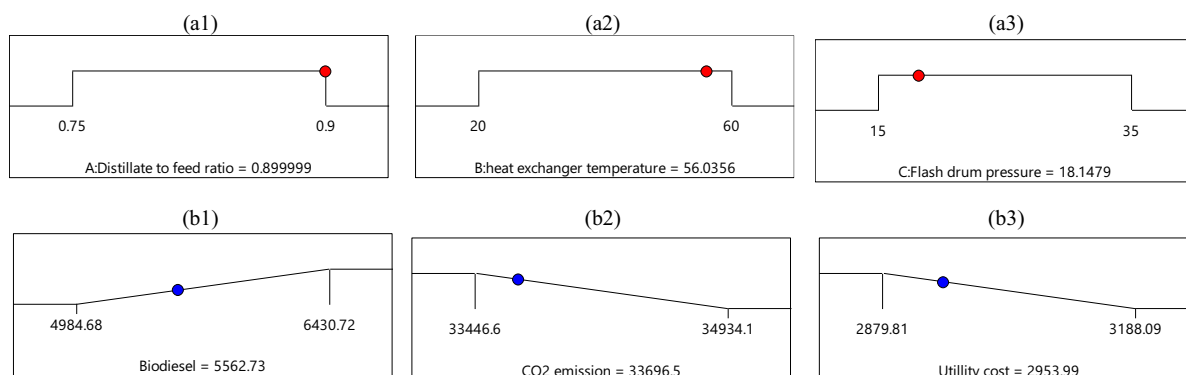

Figure 7. Desirability ramp of desirable value for input factor for (a1) distillate-to-feed ratio, (a2) temperature, (a3) pressure, and optimized output for (b1) biodiesel yield, (b2) CO_2 emission, and (b3) utility cost.
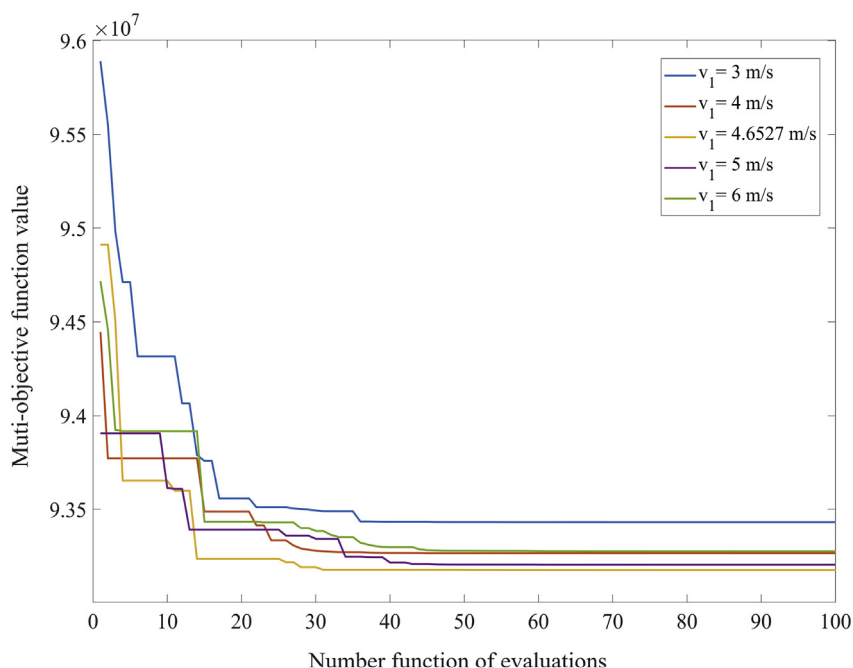

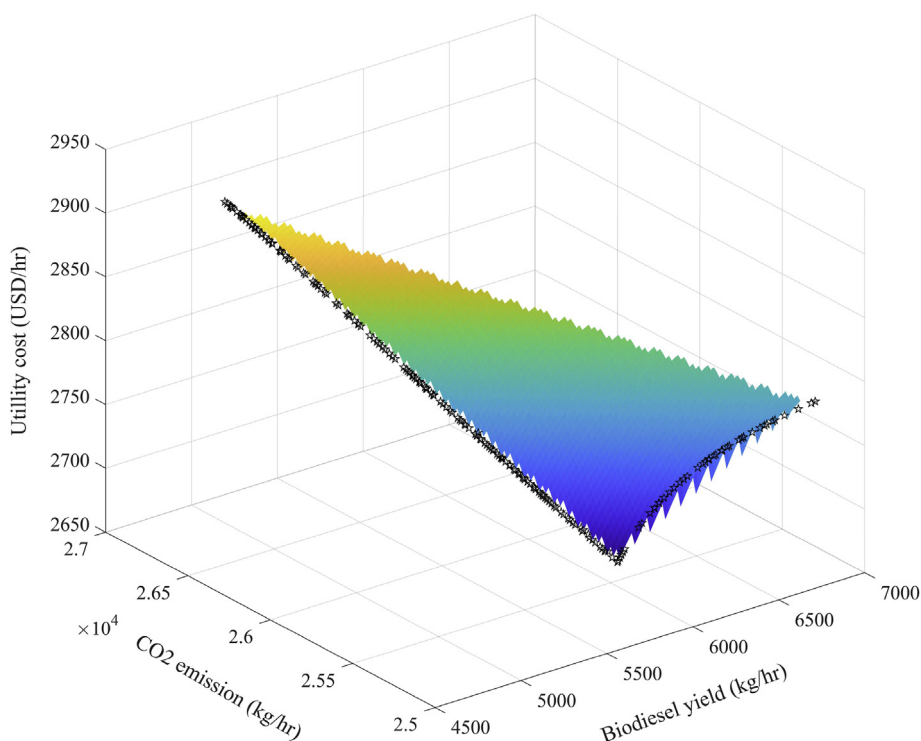Figure 8. Comparison of the convergence rate of five atom velocities.

Figure 9. 3D Pareto optimal for utility cost, biodiesel yield, and CO_2 emission.

terms of product purity, the effect was found with an adjustment in the distillate-to-feed ratio [27]. Nevertheless, increasing the heat exchanger temperature (20–60°C) had the opposite effect, lowering biodiesel production. This could be due to the hydrocarbon molecules vaporizing more quickly. Figure 5b1 and b2, the temperature of the heat exchanger rises by increasing the exothermic reaction, which is promoting the reaction of cracking heavy hydrocarbons are generated [28]. Therefore, CO_2 emissions decreased. Figure 5c1 and c2, when the temperature in the heat exchanger is raised (20 to 60 °C), the utility costs were reduced. As a result, higher temperatures reduced the distillation column's feeding rate, lowering the amount of work required by the equipment [29]. Figure 6 (a1-c2) demonstrate the relationship between simulated versus actual values and studentized residual plots for biodiesel yield (Figure 6a1 and a2), CO_2 emission (Figure 6b1 and b2), and utility cost (Figure 6c1 and c2), respectively. A higher correlation value for all responses implies that the independent and dependent variables have a good relationship.

The pressure, temperature, and distillate-to-feed ratio were kept within the boundaries of the process simulation. Simultaneously, the CO_2 emission and utility costs were minimized. Figure 7 (a1-a3) presented the optimum inputs for the distillate-to-feed ratio of 0.899999, heat exchanger temperature of 56.0356 °C, and flash drum pressure of 18.1479 bar, respectively. Figure 7 (b1-b3) showed the optimum outputs for biodiesel yield, CO_2 emission, and utility cost, respectively. The

process factors were adjusted to maximum biodiesel production. The optimum values for biodiesel yield, CO_2 emission, and utility cost were 5,562.73 kg/hr, 33,696.5 kg/hr, and 2,953.99 $/hr, respectively.

This research employed the ASO algorithm to search for the best solution by examining the ability to search and achieve the optimal solution for productivity, economic and environmental impacts. In optimization, all three decision variables were defined randomly in MATLAB V2019a before being sent as the Aspen plus V11 input; it obtained Pareto optimum after 100 iterations, 200 populations. The productivity, economic and environmental aspects had monotonically increased tendencies, which yield biodiesel increase while decreasing CO_2 emissions and utility costs. When choosing the biodiesel plant that offers the best accommodation between the examined parameters [28], this direction of optimum solution should be considered (yield of biodiesel, CO_2 emission, and utility cost). The best solution for atom velocity obtained by the ASO is $v_1 = 4.6527$, $v_2 = 4.8209$, $v_3 = 5.6803$, $v_4 = 1.1467$, $v_5 = 0.8049$, $v_6 = 2.7014$, $v_7 = 17.3687$, $v_8 = 14.2594$, $v_9 = 2.1102$, $v_{10} = 8.9323$.

Figure 8 shows a comparison of the convergence changes in the velocity of different atoms ($v_1 = 3, 4, 4.6527, 5, 6$). After 100 iterations, the convergence of the ASO showed considerable changes, especially in the early iterations. After that, the amplitude or frequency of the fluctuation declines and the atomic position became monotonous, eventually stabilizing at the top of the globe in subsequent rounds. This behavior indicated that ASO first does a global search across all search regions, then does a local search to find the area with the highest chances. Atom velocity optimization ($v_1 = 4.6527$) had the fastest convergence rate, according to the data. It is possible to bypass potential areas at a local optimal [11]. In this paper, it was demonstrated that it is a very desirable MOO approach for determining the parameters for biodiesel production.

The 3D Pareto optimal is presented in Figure 9. Each black dot represents a solution involving a distinctive design variable. Pareto solutions will improve one objective at the expense of another [30]. For example, if the operator chooses to obtain more biodiesel yield, it will be sacrificed in terms of higher reaction temperatures leading to higher costs. It can be noted that the points in the Pareto are located close to the two edges of the Pareto area. Three variables were defined: the distillate-to-feed ratio of DIESELCOL, the temperature of COOL-HDT, and the pressure of FLSH-HDT. As a result, the

Table 6. Comparison between the results of CCD and ASO optimization.

	Optimum value	
	CCD	ASO
Distillate-to-feed ratio	0.899999	0.951134
Heat exchanger temperature (°C)	56.0356	66.5025
Flash drum pressure (bar)	18.1479	41.8179
Biodiesel yield (kg/hr)	5,562.73	5,982.24
CO_2 emission (kg/hr)	33,696.55	33,247.97
Utility cost (USD/hr)	2,953.99	2,805.32

distillate-to-feed ratio was 0.698866–0.951134, the temperature between 6.36414 and 73.6359 °C and the pressure was 8.18207–41.8179 bar. Thus, biodiesel yield increased with higher distillate-to-feed ratio, temperature, and pressure in Pareto-optimal solutions. Moreover, they were increasing distillate-to-feed ratio, temperature, and pressure, reducing CO_2 emission and utility cost. The results show Pareto-optimal solutions in 200 runs, including 5,001.42 to 6,819.96 kg/hr for biodiesel yield. Furthermore, CO_2 emission were 34,485.82 to 32,801.56 kg/hr. Moreover, utility cost was 2,986.73 to 2,766.55 USD/hr.

When using the distillate-to-feed ratio of 0.951134, the temperature of 66.5025 °C, and the pressure of 41.8179 bar, the optimum point from the Pareto optimal solution with the largest biodiesel yield, the lowest CO_2 emission, and the lowest utility cost was chosen. Table 6 shows a comparison of the optimum values. When comparing the optimum value of CCD with ASO, it was found that ASO could reduce CO_2 emissions by 1.33% and reduce utility costs by 5.03% while increasing biodiesel yield by up to 7.01%.

4. Conclusions

The RSM and MOO were used in cooperation with the central composite. The CCD is limited to producing second-order equations, which means it cannot be utilized to optimize all procedures. ASO algorithms can also be optimized to a special problem, leading in higher efficiency and convergence than the CCD. Thus, we chose a final solution from among the Pareto optimal solutions due to having the balance of objective functions in consideration including productivity, economic, and environmental aspects. ASO is used for successful modelling and optimizing biodiesel yield production. Considering a specific optimum solution to explore biodiesel yield maximization, minimizing utility cost, and minimizing CO_2 emission, an optimal point among the Pareto front was found. MOO employing the ASO provides Pareto-optimal solutions. This method provides Pareto optimal solutions to get a final optimum solution. The ASO can reduce CO_2 emissions by 1.33%, lower utility costs by 5.03%, and increase biodiesel yields by 7.01% when comparing optimal CCD values with ASO. It was concluded that the ASO algorithm could optimize the distillate-to-feed ratio, heat exchanger temperature, and the flash drum pressure within the boundary of the variables to minimize the objective function.

Declarations

Author contribution statement

Rawinun Junsittiwate: Conceived and designed the experiments; Performed the experiments; Analyzed and interpreted the data; Contributed reagents, materials, analysis tools or data; Wrote the paper.

Thongchai Rohitatisha Srinophakun: Conceived and designed the experiments; Analyzed and interpreted the data.

Somboon Sukpancharoen: Conceived and designed the experiments; Analyzed and interpreted the data; Wrote the paper.

Funding statement

Data availability statement

Data associated with this study has been deposited at https://drive.google.com/drive/u/0/folders/1XpHyfQd6IRVzTh8DC0XqNTHDA5-sza8N.

Declaration of interests statement

The authors declare no conflict of interest.

Additional information

No additional information is available for this paper.

References

[1] Agricultural statistics of Thailand 2020, Office of agricultural economics, Available at: https://www.oae.go.th/assets/portals/1/files/jounal/2564/yearbook2563.pdf. Accessed May 2021.

[2] M. Belna, A. Ndiaye, F. Taillandier, L. Agabriel, A.-L. Marie, G. Gésan-Guiziou, Formulating multi-objective optimization of 0.1 μm microfiltration of skim milk, Food Bioprod. Process. 142 (2020) 244–257.

[3] H. Shahbeig, M. Nosrati, Pyrolysis of municipal sewage sludge for bioenergy production: thermo-kinetic studies, evolved gas analysis, and techno-socio-economic assessment, Renew. Sustain. Energy Rev. 119 (2020) 109567.

[4] X. Xin, K. Dell, I.A. Udugama, B.R. Young, S. Baroutian, Transforming biomass pyrolysis technologies to produce liquid smoke food flavoring, J. Clean. Prod. 294 (2021) 125368.

[5] N. Taghili, M. Manteghian, A. Jafari, Novel preparation of MoO3/γ-Al2O3 nanocatalyst: application in extra-heavy oil visbreaking at atmospheric pressure, Appl. Nanosci. 10 (2020) 1603–1613.

[6] S. Sukpancharoen, P. Hansirisawat, T.R. Srinophakun, Implementation of response surface to optimum biodiesel power plant derived from empty fruit bunch, J. Energy Resour. Technol. 144 (1) (2021) 12101.

[7] M. Colakoglu, A. Durmayaz, Energy, exergy and environmental-based design and multi-objective optimization of a novel solar-driven multi-generation system Energy, Convers. Manag. 227 (2021) 113603.

[8] S. Sukpancharoen, T.R. Srinophakun, P. Aungkulanon, Grey Wolf Optimizer (GWO) with Multi-objective optimization for biodiesel production from waste cooking oil using Central Composite Design (CCD), Int. J. Mech. Eng. Robot. Res. 9 (8) (2020) 1219–1225.

[9] S. Sukpancharoen, Application of Spotted Hyena Optimizer in cogeneration power plant on single and multiple-objective, in: IEEE CCWC, 2021, pp. 1–5.

[10] W. Zhao, L. Wang, Z. Zhang, A novel atom search optimization for dispersion coefficient estimation in groundwater, Future Generat. Comput. Syst. 91 (2019) 601–610.

[11] M.A. Almagboul, F. Shu, Y. Qian, X. Zhou, J. Wang, J. Hu, Atom search optimization algorithm based hybrid antenna array receive beamforming to control sidelobe level and steering the null, AEU-Int. J. Electron. Commun. 111 (2019) 152854.

[12] A.M. Agwa, A.A. El-Fergany, G.M. Sarhan, Steady-state modelling of fuel cells based on atom search optimizer, Energies 12 (10) (2019) 1884.

[13] S. Bhattacharya, Chapter 2 central composite design for response surface methodology and its application in pharmacy, Res. Surf. Methodol. Eng. Sci. (2021).

[14] E.O. Ajala, A.B. Ehinmowo, M.A. Ajala, O.A. Ohiro, F.A. Aderibigbe, A.O. Ajao, Optimisation of CaO-Al2O3-SiO2-CaSO4-based catalysts performance for methanolysis of waste lard for biodiesel production using response surface methodology and meta-heuristic algorithms, Fuel Process. Technol. 226 (2022) 107066.

[15] M.B. Shemfe, S. Gu, P. Ranganathan, Techno-economic performance analysis of biofuel production and miniature electric power generation from biomass fast pyrolysis and bio-oil upgrading, Fuel 143 (2015) 361–372.

[16] S. Kerdsuwan, K. Laohalidanond, Renewable energy from palm oil empty fruit bunch, Renew. Energy - Trend. Appl.: Intech (2011) 123–150.

[17] J.F. Peters, S.W. Banks, A.V. Bridgwater, J. Dufour, A kinetic reaction model for biomass pyrolysis processes in Aspen Plus, Appl. Energy 188 (2017) 595–603.

[18] J. Sadhukhan, K. Siew Ng, Economic and European union environmental sustainability criteria assessment of bio-oil-based biofuel systems: refinery integration cases, Ind. Eng. Chem. Res. 50 (2011) 6794–6808.

[19] R. Junsittiwate, T.R. Srinophakun, S. Sukpancharoen, Techno-economic, environmental, and heat integration of palm empty fruit bunch upgrading for power generation, Energy Sustain. Dev. 66 (2022) 140–150.

[20] T. Keller, J. Holtbruegge, A. Górak, Transesterification of dimethyl carbonate with ethanol in a pilot-scale reactive distillation column, Chem. Eng. J. 180 (2012) 309–322.

[21] F. Abnisa, W.M.A. Wan Daud, J.N. Sahu, Optimization and characterization studies on bio-oil production from palm shell by pyrolysis using response surface methodology, Biomass Bioenergy 35 (8) (2011) 3604–3616.

[22] D. Madathil, R. Pandi Va, M.G. Nair, T. Jamasbb, T. Thakur, Consumer-focused solar-grid net zero energy buildings: a multi-objective weighted sum optimization and application for India, Sustain. Prod. Consum. 27 (2021) 2101–2111.

[23] Z. Boubacar Laougé, A. Seyhan Çığgın, H. Merdun, Optimization and characterization of bio-oil from fast pyrolysis of Pearl Millet and Sida cordifolia L. by using response surface methodology, Fuel 274 (2020) 117842.

[24] L. de Souza Guedes, I. Cristina Sales Fontes Jardim, L. Vilela de Melo, M. Massumi Beppu, Study of the effect of the operating parameters on the separation of bioactive compounds of palm oil by ultra-high performance supercritical fluid chromatography using a design of experiments approach, Can. J. Chem. Eng. (2017) 1–38.

[25] V. Sakhre, Reactive distillation: modeling, simulation, and optimization, Model. Simulat. Opti. (2019).

[26] S. García-Alonso, R.M. Pérez-Pastor, A. Garcıa-Alvarez, F.J. Garcıa-Frutos, An approach to uncertainty estimation in determining polycyclic aromatic hydrocarbons in fuel-contaminated soils, Toxicol. Environ. Chem. 95 (1) (2013) 26–37.

[27] B.J. Abukari, K.B. Pelig-Ba, Optimization using central composite design (CCD) of response surface methodology (RSM) for biosorption of hexavalent chromium from aqueous media, Appl. Water Sci. 10 (2020) 135.

[28] R.K. Singha, D.K. Shrivastavab, A. Sarkara, J.P. Chakraborty, Co-pyrolysis of eucalyptus and sodium polyacrylate: optimization and synergistic effect, Fuel 277 (2020) 118115.

[29] I. Juan, P. Páez, S. De-León Almaraz, A. Román-Martínez Sustainable wastewater treatment plants design through multi-objective optimization, Comput. Chem. Eng. 140 (2020) 106850.

[30] A.-D. Li, Z. He, Multi-objective feature selection for key quality characteristic identification in production processes using a nondominated-sorting-based whale optimization algorithm, Comput. Ind. Eng. 149 (2020) 106852.

[31] S. Sukpancharoen, B. Prasartkaew, Combined heat and power plant using a multi-objective Henry gas solubility optimization algorithm: a thermodynamic investigation of energy, exergy, and economic (3E) analysis, Heliyon 7 (9) (2021), e08003.